Available online at www.sciencedirect.com

SCIENCE DIRECT®

Journal of Marine Systems 55 (2005) 47–66

JOURNAL OF MARINE SYSTEMS

www.elsevier.com/locate/jmarsys

Initial spread of an effluent and the overturning length scale near an underwater source in the northern Adriatic

Vlado Malačič*

Marine Biology Station, National Institute of Biology, Piran, Slovenia

Received 21 February 2004; accepted 9 July 2004
Available online 6 October 2004

Abstract

The rise of an effluent emerging from the diffusers of the submarine sewage outfall of a small town (15000 PE) is numerically simulated with a model of initial dilution. Results were evaluated using the vertical distribution of faecal coliforms that were analyzed for two field surveys at the central position. In addition to that, the overturning length scale was calculated from vertical profiles of temperature, salinity and density. These were obtained from two autumn surveys using fine-scale CTD casts in the sewage near-field around the diffusers which lie on a flat seabed in a shallow sea. Indications that a turbulent effluent could manifest itself with a local maximum of the overturning length scale are discussed. The depth of the subsurface local peak of the overturning length scale, calculated from the density profile in the core of the sewage near-field, matches the position of the peak of the vertical distribution of faecal coliforms and the height of the simulated plume rise. The 3D space distribution of the overturning length scale indicates a structure with enhanced overturning activity below the surface mixed layer over an area of 1 km^2 which could be attributed to an effluent that erupts turbulently from diffusers.

Keywords: Coastal oceanography; Sewage dilution; Overturning length scale; Adriatic sea; Gulf of Trieste

1. Introduction

Studies that were conducted decades ago (Avčin et al., 1979; Faganeli, 1982; Malej, 1980) did not detect the severe deterioration of the ambient fluid around the single diffuser of the outfall of Piran (a small town), in Slovenia. The sampling method then was of poor vertical resolution and there was only a modest chance of catching the layer of polluted water. In a study of the spread of sewage from two submarine diffusers that was conducted from 1996 to 1999, the sewage near-field was surveyed with a CTD probe in a very shallow sea (depth 21 m). The hydraulics of the discharge system were also studied, (Malačič, 2001) because the flow rates and buoyancy fluxes through the orifices of the diffusers are the initial conditions for the modelling of the initial dilution of sewage in the sea, after which the secondary dilution, which also

* Fax: +38 6 5 671 2902.
E-mail address: Malacic@mbss.org.

0924-7963/$ - see front matter © 2004 Elsevier B.V. All rights reserved.
doi:10.1016/j.jmarsys.2004.07.017

depends on advection, could be estimated (Malačič et al., 2000a).

Analysis of water samples for faecal coliform bacteria and nutrients at one representative (central) station was also performed. From six surveys during 1997–1999, eight nutrient compounds were analyzed (NO_3^-, NO_2^-, NH_4^+, ΣN_{in}, PO_4^{3-}, SiO_4^{4-}, N-tot, P-tot). The analysis showed that only ammonia followed the increase of bacteria (Mozetič et al., 1999) in a layer of neutral buoyancy, with a correlation factor of 0.58. There was no significant correlation between bacteria and fluorescence, nor with dissolved oxygen. Fluorescence showed a patchy distribution of Chlorophyll-*a* above the diffusers during the winter period (Malačič and Vukovič, 1997) when the water column was almost homogeneous. Small wiggles on the vertical profiles of temperature and salinity, which also resulted in density fluctuations, were observed on vertical CTD profiles that were followed in real time. Many of them could not be explained simply by temperature and conductivity mismatch due to the different dynamic responses (UNESCO, 1988) of the probes.

Intensified temperature and salinity fluctuations at certain depths in vertical casts look similar to those observed elsewhere using a variety of different CTD probes, mostly microstructure probes. However, the mechanisms that cause these small vertical fluctuations of density include surface wave breaking (Oakey and Elliott, 1982), internal waves (Dillon, 1982), wind-driven Langmuir cells (D'Asaro and Dairiki, 1997) over the ocean, patchy turbulent mixing at the thermocline (Etemad-Shahidi and Imberger, 2001), intrusions and underflows of a denser river fluid (Imberger and Hamblin, 1982), as well as slope turbulent gravity currents and episodic convective plumes (Fer et al., 2002), and surface cooling and convection overturns (Brubaker, 1987). Different turbulent processes at the sea-surface (Thorpe, 1995) expand deeper into a water column and a shallow sea may be overwhelmed by them on particular occasions. In this work, the effects of convection and diffusive convection on the overturning scale will be presented, together with the possibility of the influence of an alien turbulent effluent.

The setup of an onboard sampling procedure, through which a thin layer of diluted sewage water with enhanced bacteria content is to be detected, is a time-consuming process, and moreover, an uncertain one, unless the fluid in this layer differs significantly in a property that is easily measured on board. This could be achieved by measurements of turbidity, PAR and fluorescence (Petrenko et al., 1997; Washburn et al., 1992; Wu et al., 1994), or through a more complicated method using a dye, like Rhodamine B (Sherwin and Jonas, 1994), together with spores of *Bacillus globigii*. (Sherwin et al., 1997). However, observations around the diffusers in question showed that the fluorescence signal is not a distinctive one for the sewage discharged from the outfall in Piran, nor are dissolved oxygen or PAR (Malačič and Vukovič, 1997).

The numerical model of the initial dilution and rise of an effluent from an orifice of a diffuser was developed for a complicated vertical profile of density. It was tested, however, on simple linear stratification with previous analytical solutions (Malačič, 2001). The model was applied in planning for future discharges (Malačič et al., 2000a). In this work, the model results will be applied to real stratified conditions in order to detect faecal coliforms in the coastal sea.

Field campaigns revealed that a layer in which sewage spreads horizontally could hardly be traced with a conventional CTD, without a die release, or without a time-consuming sampling technique to analyze the near-field for chemical substances (ammonia). The need for quick detection of this layer with a simple CTD cast emerged. For this reason, past CTD surveys were reviewed again in order to apply the overturning length scale (l_T), first introduced in the 1970s (Thorpe, 1977), which measures the vertical extent of the overturning vortices that would be acquired by water parcels in order to find their statically stable position. It was later shown (Dillon, 1982) that l_T is proportional to the Ozmidov length scale $l_o=(\varepsilon/N^3)^{1/2}$, where ε is the dissipation rate of kinetic energy, and N is the buoyancy frequency near the surface in the wind-driven mixed layer. The Ozmidov scale measures the thickness of a fluid in which the buoyancy force is balanced by the inertial force. Dillon found a match between the two scales $l_o=0.8l_T$, that holds well for nearly three orders of magnitude in the ocean, as well as in lakes at the base of the mixing layer and thermocline. Both Thorpe and Dillon were calculating the overturning length scale from the vertical profiles of temperature.

While it seems that there are no applications of the overturning length scale in studies of the spread of turbulent jets in a natural ambient, there are laboratory experiments (Fonseka et al., 1998) where the evolution and collapse of a turbulent blob is studied. The blob emerged horizontally as a jet from a nozzle in a stratified fluid in a lab container, and after a time $t \cong 4.5/N$, the blob attained the maximum thickness that is proportional to l_T, after which stratification squeezed the blob vertically into a planar dipole. Another laboratory study (Flór et al., 1994) also applied l_T and correlated it with the height of a turbulent patch in a two layer fluid into which a volume of fluid with neutral buoyancy was horizontally injected. Density fluctuations were similar to those that were observed in the sea above the sewage diffusers.

2. Study area

2.1. Location, discharge conditions and field survey

The field campaigns were performed at the southern part of the Gulf of Trieste (Fig. 1), where the bottom is reasonably flat and its depth varies with tides between 20.5 and 21.5 m. The sewage system of the town of Piran composes only 7% of the sewage load that arrives in the Gulf of Trieste (Olivotti et al., 1986). Two pipelines, one of length 3.25 km and of internal diameter 0.59 m, and the other of length 3.65 km and of internal diameter 0.375 m, were laid 1 m above the sea-floor. Sewage flows though them gravitationally from a treatment plant on land. The pipes end with diffusers that have orifices of 0.1 m in diameter every 10 m, drilled on alternate sides of the

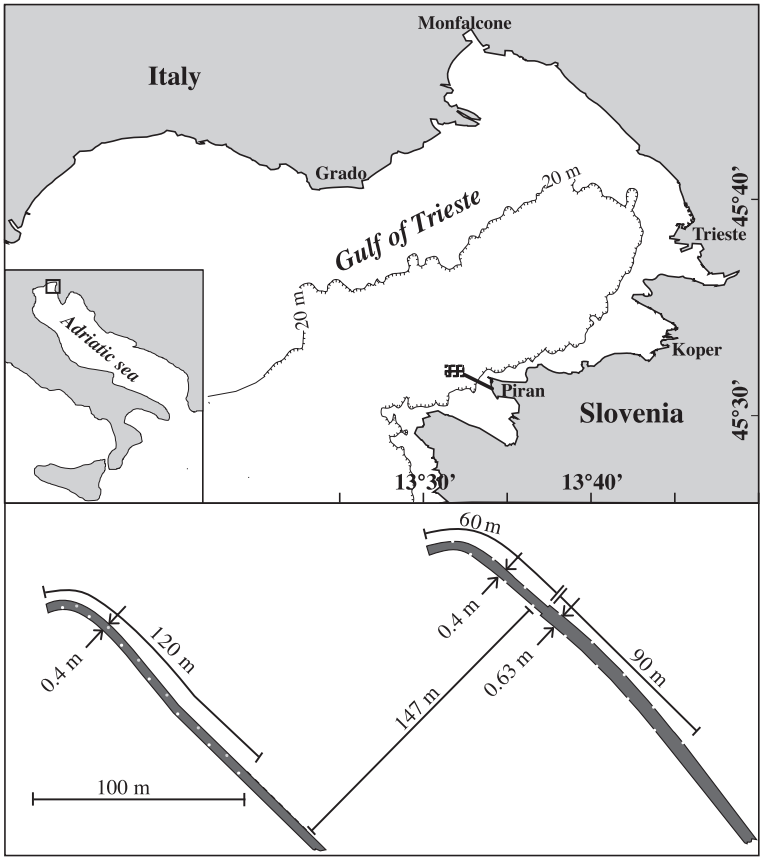

Fig. 1. Location map (top) of the sewage outfall at the southern side of the entrance to the Gulf of Trieste. There are actually two parallel pipelines that end with diffusers (bottom), which were deflected westward at the time of the CTD surveys (1996–1998). Diffusers are 2.6 km away from the nearest land point, the tip of the cape (Malačič, 2001).

diffusers. Details about the geometry of the discharge system and related hydraulics are described elsewhere (Malačič, 2001).

There are two daily peaks of the discharge rate, one around 10 AM, and the other at 10 PM (Malačič, 2001), when the water consumption of the town is increased. The time that sewage takes to reach the diffusers from the power plant through the two pipes is estimated to be around 2 h, depending on the flow rate. We can estimate the flux of sewage from a single side orifice of diameter 0.1 m of the diffuser which then serves as an input parameter in a model of the initial dilution of effluent that spreads in an environment with a known vertical density profile. During field surveys, the flow rate through both pipes was 97.6±20.7 l/s on 26 September 1997, and 166.3±22.7 l/s on 12 October 1998. The ratio of flow rates between the smaller pipe, which ended at that time with a diffuser with seven operative orifices, and the larger pipe with a diffuser of 18 orifices was around 0.3 (Malačič, 2001). This yields for the outflow velocity through an orifice a value of 0.45±0.09 m/s for the first survey, and of 0.8±0.2 m/s for the second survey. In numerical simulations of initial dilution, these variations of initial outflow velocity are taken into consideration. The Reynolds number of a jet near an orifice is therefore around 5×10^4, when u_0=0.5 m/s is chosen for the outflow velocity. The density of an effluent at the place of discharge does not vary much, and we may reasonably suppose for it a constant value of 1000 kg/m^3 in both surveys. Major variations are those of the ambient density ρ_a.

Fig. 2 shows the positions of the two diffusers and a planned grid of CTD stations above them that covers an area smaller than 1×1 km. The grid of stations was made simple for easier vessel maneuvering. Stations are separated by 0.1′ (185 m) in S–N direction, and 0.1′ (130 m) in E–W direction. The 9.5-m-long vessel was positioned at each station using a GPS system, the position resolution was then estimated to be around 35 m by following the fluctuation of position on several occasions. The vessel stayed at each station for about 3 to 7 min and was not anchored.

Samples for bacterial analysis were taken at the central station just after the CTD survey of 31 stations. The latter took less than 2.5 h, while the former about 0.5 h. Temperature, salinity and density profiles were inspected visually on board. At depths where small-

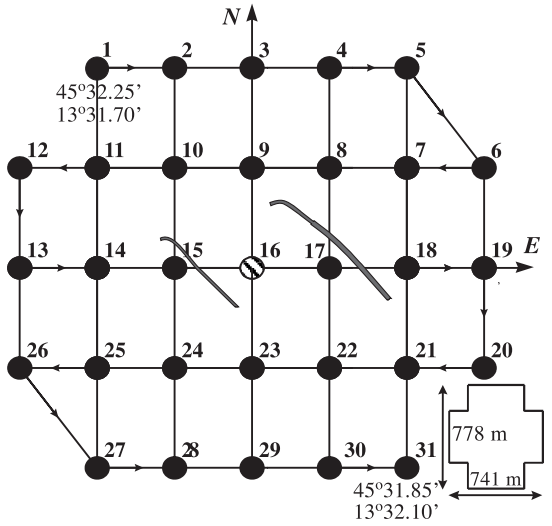

Fig. 2. Idealized grid of stations of CTD casts around the diffuser. Stations are 0.1′ apart eastward, as well as northward, which it was possible to determine with ordinary GPS navigation. The position accuracy was estimated to 25–35 m. In windy weather, maneuvering and on board work was difficult without anchoring above the diffusers, and the actual grid of stations (see Fig. 9) is quite different from this one. CTD profiles were usually completed within 2 h of each cruise and were performed mostly during the slack tide period.

scale wiggles were detected (around a depth of 16 m), the effluent was expected, but its presence was not confirmed by on board measurements. The water was pumped from different depths and samples were analyzed in the laboratory for faecal coliform bacteria. They were filtered through 0.45 μm pore-sized filters and incubated on an m-FC agar medium at 44.5±0.2 °C for 24 h (Mozetič et al., 1999).

Tides in this area are of a mixed type, well represented by seven constituents, four semidiurnal and three diurnal (Malačič et al., 2000b). Tidal currents mostly follow the standing wave pattern, their amplitude is of 0.09 m/s during spring tides, when the tidal range is of 1 m (Malačič and Viezzoli, 2000). Both field works were conducted during the period of slack tides over less than 2 h.

2.2. Weather conditions

Winds in the area are mostly of two types, the most frequent are the ‘bora’ wind (ENE) and ‘sirocco’ or ‘jugo’ wind that blows from the south. The Bora is more frequent during the winter period, more gusty and energetic (monthly mean speed 5.0 m/s) than the

jugo which has a monthly mean speed between 3.0 and 4.4 m/s (Ogrin, 1995). This was later confirmed by the wind measurements on a coastal buoy, just 2 km from the sewage diffusers in a NE direction.

On the morning of 26 September 1997, the cruise took place after several days of bora wind, that had significantly mixed the water column. Forced mixing was supported by the bora wind that was still blowing on that day. Records of on board measurements of wind show that the instantaneous wind speed ranged between 6 and 11 m/s during the few hours of the field survey. The meteorological station of the Hydrometeorogical Institute of Slovenia at the nearby airport, 9.8 km away from the diffusers in a SE direction, recorded a rapid increase of air temperature: from 12.9 °C at 8:00 local time to 19.1 °C at 10:00, while relative humidity decreased from 65% to 49% in the same time interval.

The second survey was conducted on a cloudy morning, 12 October 1998, in calm weather conditions. The southern wind was of a speed lower than 3.0 m/s. The air–temperature increase was from 13.3 °C at 7:30 AM to 14.5 °C at 9:30 AM, while the relative humidity was high and steady at that time, between 95% and 97%. The previous 2 weeks were rainy and there was a strong autumn peak of river Po discharge. There are, however, five Italian rivers to the north of it, like Isonzo (or Soča) that is just 22 km northward from the place of the field survey.

3. Methods

3.1. The fine-scale CTD instrument

The fine-scale CTD was designed by the University of Western Australia for ecological field work. The CTD gives a finer vertical resolution of the temperature and salinity structure of the water column than most standard probes (Anon., 1992). The probe (Fig. 3) is a free-falling one with a speed of around 1 m/s. Recent tests have shown that regardless of the stratification, the probe has such an inertia that the final vertical speed of the probe is reached at depths between 4 and 5 m. The sampling period of all parameters that are measured is 50 Hz, which yields the average vertical space resolution of a CTD profile of 2.5 cm, and the accuracy of the pressure sensor

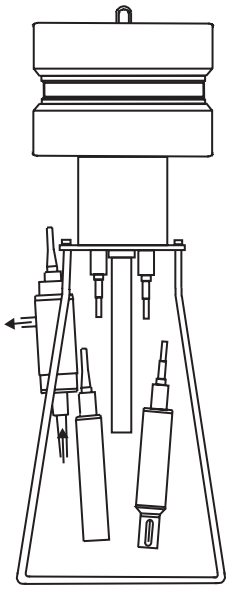

Fig. 3. Scheme of a free-falling fine-scale FPS2 probe. The probe is about 1 m in height and has 35 kg of mass with buoyant floats on top that surround the electronics in the cylinder, below which is a pump on the left hand side that drives the water through the conductivity and oxygen probe. Sensors are placed within the stainless steel conical cage further below. The scheme is simplified for clarity, but the probe carries the Seabird sensors—temperature (SBE 3-01/F), conductivity (SBE 4-01/0) and oxygen (SBE-13 with Beckman polarographic element)—as well as a Digiquartz 0–60-m pressure sensor (of resolution of 2 mm), and the Minitracka fluorometer of Chelsea Instruments.

(Paroscientific Digiquartz pressure sensor, depth 0–60 m) is around 2×10^{-3} m. Since each cast lasts for about 22 s (the depth shallower than 22 m), it is estimated that the horizontal drift of the probe (vessel) within this time is smaller than 25 m under a wind speed below 6 m/s. The probe is designed to measure temperature, conductivity, dissolved oxygen and fluorescence only during the falling phase.

The sensitivity of the probe under free-falling operation was studied more than a decade ago in a vertical tank, filled with different ‘double layer’ fluids (Vollmer, 1991). The dynamic responses of the temperature, conductivity and oxygen sensors were thoroughly examined. The match of the temperature sensor SBE and the pumped conductivity sensor SBE 4 followed research that resulted in a smoothing/sharpening software elaboration of the CTD profile that is grounded on a complex Z-transform of the sensors’ output (Fosdar et al., 1985). The goal was to increase

the sensors' sensitivity in the mid-frequency range, and to decrease noise amplification by low-pass filtering in the high-frequency range (above 20–30 Hz).

3.2. Numerical model of initial dilution

The model supposes that the turbulence of the ambient sea is insignificant compared to the turbulence of the emerging sewage water and that the mass and volume fluxes of a discharge are constant during the uplift of a plume. The former condition is difficult to meet in the sea, while the latter is easy, since the time in which the buoyant plume would reach the sea-surface or a buoyantly neutral layer is never longer than one minute. The model ('SplinRun') is described in detail elsewhere (Malačič, 2001), where model sensitivity to initial conditions and model calibration were determined. Here it will be only briefly summarized. The dilution in the plume is parametrized through the entrainment process, in which the volume flux ϕ changes along the trajectory $s(t)$ of the plume's core due to entrainment of ambient fluid through the plume's side surface (Turner, 1986), which has a perimeter of $2\pi b$ and a height of ds:

$$\frac{\mathrm{d}\phi}{\mathrm{d}s} = E = 2\pi b\alpha u(s), \tag{1}$$

b is the radius at which the velocity falls to 1/e of the axis value, the entrainment parameter α ($\cong 0.08$) is the first model parameter, and $u(s)$ is the peak velocity at the center of a plume's slice. The problem simplifies if the Gaussian variations of the velocity $u(r,s)$ and of the density deficit $\Delta\rho$ ($=\rho_a-\rho$) across the buoyant slice are supposed, where $\rho_a=1000.0+\sigma_T$ is the ambient density:

$$u(s,r) = u(s)\mathrm{e}^{-r^2/b^2};\ \Delta\rho(s,r) = \Delta\rho(s)\mathrm{e}^{-r^2/\lambda^2 b^2}, \tag{2}$$

where a second model parameter λ has been introduced. From numerous observations, it was determined (Fischer et al., 1979) that the cross-section profile of the density deficit is wider than the profile of velocity and $\lambda \cong 1.2$. In the Bay of Piran, the sewage plume that emerges from an orifice 0.1 m in diameter reaches a radius b of the order of a few meters before reaching a layer of neutral buoyancy or the sea-surface. The rate of change of volume flux, radial and vertical components of momentum flux, and of buoyancy flux can be written in terms of core velocity u, plume's radius b, angle of inclination of a tangent of a plume's trajectory to the horizontal axis θ, and of the core density deficit $\Delta\rho$ (Fischer et al., 1979)

$$\frac{\mathrm{d}(ub^2)}{\mathrm{d}s} = 2\alpha bu, \tag{3}$$

$$\frac{\mathrm{d}(u^2b^2\cos\theta)}{\mathrm{d}s} = 0, \tag{4}$$

$$\frac{\mathrm{d}(u^2b^2\sin\theta)}{\mathrm{d}s} = \frac{2g\Delta\rho}{\rho_{a0}}\lambda^2 b^2, \tag{5}$$

$$\frac{\mathrm{d}(\Delta\rho ub^2)}{\mathrm{d}s} = \frac{(1+\lambda^2)}{\lambda^2}ub^2\frac{\mathrm{d}\rho_a}{\mathrm{d}s}. \tag{6}$$

These are four variables that change along the plume's path s, where the constant $\rho_{a0}=\rho_a$ (s=0) is the ambient density near the orifice. This system is transformed into a system of explicit coupled non-linear equations (Featherstone, 1984)

$$\frac{\mathrm{d}u}{\mathrm{d}s} = \frac{2g\lambda^2\Delta\rho}{\rho_{a0}u}\sin\theta - \frac{2\alpha u}{b}, \tag{7}$$

$$\frac{\mathrm{d}b}{\mathrm{d}s} = 2\alpha - \frac{g\lambda^2\Delta\rho b}{\rho_{a0}u^2}\sin\theta, \tag{8}$$

$$\frac{\mathrm{d}\theta}{\mathrm{d}s} = \frac{2g\lambda^2\Delta\rho}{\rho_{a0}u^2}\cos\theta, \tag{9}$$

$$\frac{\mathrm{d}\Delta\rho}{\mathrm{d}s} = \frac{(1+\lambda^2)}{\lambda^2}\frac{\mathrm{d}\rho_a}{\mathrm{d}z}\sin\theta - \frac{2\alpha\Delta\rho}{b} \tag{10}$$

that is solved using the Runge–Kutta method with an adaptive step in the model. This means that the vertical density gradient dρ_a/dz at an arbitrary height at which there were no measurements of the density ρ_a, needs to be known. The density ρ_a and dρ_a/dz were provided at each step by the cubic spline interpolation method (Press et al., 1992) from pairs (z_i, ρ_{ai}), where ρ_{ai} is the 'measured' density at a height of z_i. Additional variables that are monitored along the integration of this system are the coor-

dinates (x, z) of the plume's core, where dx/ds=cos θ and dz/ds=sin θ, and the dilution along the path of the plumes' center (Fan and Brooks, 1966)

$$S_{\mathrm{n}}(s) = \frac{4\lambda^2 u(s) b^2(s)}{(1+\lambda^2) u_0 d^2}, \tag{11}$$

where the subscript n indicates numerical dilution.

The integration of the system starts near the orifice, at a distance s_0=6.2d, where d is the diameter of the orifice (Featherstone, 1984). At this distance, the zone of established flow starts. The initial velocity at s=s_0 is the same as the mean exit velocity at the orifice $u(s_0)$=u_0=4ϕ_0/(πd^2) and the initial plume's radius follows from the conservation of momentum flux b_0=d/$2^{1/2}$. The initial tilt of a buoyant plume is prescribed with the angle of the orifice θ_0, here supposed to be zero (horizontal ejection of a plume). The initial density difference $(\Delta\rho)_0$ at s=s_0 must be expressed with the difference of densities ($\rho_{\mathrm{a}0}-\rho_0$) at the orifice, where ρ_0=1000.0 kg/m^3 is the density of an effluent at the orifice. It can be shown (Malačič, 2001) that $(\Delta\rho)_0$=($\rho_{\mathrm{a}0}-\rho_0$)(1+$\lambda^2$)/(2$\lambda^2$), leading to the initial dilution S_0=2λ^2/(1+λ^2). The initial position of a plume's core is x_0=$s_0$cosθ_0, z_0=$s_0$sinθ_0.

There are two possibilities for when to stop the model simulation. One is to stop the model run as soon as the density difference $\Delta\rho$ changes sign, passing through the level of neutral buoyancy. However, at that point, the model is not near singularity and can simulate the plume's further rise due to inertia. The path of a plume's rise can be followed up to the point where the core velocity u changes sign. Only those results of a simulation are considered that do not have a change in the sign of the core velocity. At that instant, the plume's radius starts to increase rapidly and the model blows up (Malačič, 2001).

3.3. Overturning length scale

The paths that a fluid particle may follow in attaining its neutral position while keeping its own density unchanged are manifold, and the vertical extent of this migration (displacement d) is questionable in those parts of the water column that are well mixed. The maximum vertical extent of the potential migration of fluid particles is, however, bounded by the thickness of a mixed layer. Since the goal was to design a simple straightforward method for detection of an effluent, a standard sorting procedure was used (Press et al., 1992) for the vertical profile of displacements that relies on the bubble sort method with the number of operations proportional to $N\log_2 N$, where N is the number of particles with known temperature, salinity and density. In calculations performed on salinity and density profiles, artificial fluid parcels were ordered by depth in such a way that salinity and density increased with depth, while for the temperature profiles the sorting method was reversed. The temperature of fluid parcels increased with height, which is commonly found in lakes and open oceans, where vertical variations of salinity play a minor role (Dillon, 1982; Thorpe, 1977). The height is measured from the reference depth near the sea-floor. For the temperature profile d_i=z_{Si}−z_i, where z_i is the original height of a fluid particle with temperature T_i, and z_{Si} the height after the sorting procedure, while for the density and salinity profiles d_i=−h_{Si}+h_i, where h_i is the original depth of a fluid particle with salinity S_i and density σ_{Ti}, and h_{Si} is its final depth after sorting. Temperature, salinity and density values were rounded to the third decimal and only those data records in which the depth (pressure) increased over time during the drop of the probe were selected for further processing.

If the rms value l_{T} of the overturning length scale is calculated from a layer thickness Δz that captures large overturns, then turbulence having these larger scales could be characterized by the Richardson number (Zhang, 1994). On the other hand, if Δz is too large, then the details of the internal structure of turbulence are lost, i.e. separate patches of turbulence could be smeared together into one. However, dimensions of the temperature probe and of the conductivity cell also play a role since these two sensors are placed vertically and the water is passing by them during the free-fall. Since the vertical resolution of the data acquisition (2.5 cm) is high enough, and since the dimension of the temperature probe SBE-3 is of 4 cm, it remains that the dimension of the conductivity SBE-4 cell of a length of 11 cm is the dominant factor in estimating the lower limit of the averaging interval Δz. On the other hand, the water column is, in our case, of a small vertical extent (21–22 m) and if a major part of it is well mixed, which was the case during the first survey, then this

implies that Δz should be much smaller than 15 m. Since the observed pycnocline(s) are thinner than 1 m, processes around it should be captured by averaging over Δz of less than 1 m.

This lead us to test the rms of the displacements, that is, the overturning length scale L_T, using a two-step procedure for all three profiles of temperature (T), salinity (S) and density excess (σ_T). Firstly, the averaging of T, S and σ_T profiles was conducted over the averaging interval Δz_a, which ranges from a very small value (=0.001 m, no averaging) to 1.0 m. Secondly, the rms values L_T were calculated from displacements obtained from the first step, where Δz_L ranged from 0.25 up to 1 m. There were no qualitative differences found within the variety of these parameters, except that when Δz_a was larger than Δz_L a slight shift in the vertical position of the peak of L_T was observed and that when both Δz_a and Δz_L had larger values, peaks were broadened and the vertical profile smoothed, as expected. Therefore, only results for Δz_L=0.25 m will be described.

4. Results

4.1. Ambient stratification

Since during the bora wind episode on 26 September 1997, the sea-surface temperature at 0.5-m depth was between 25.88 and 26.01 °C (and salinity between 36.54 and 36.69 PSU), much higher than the air–temperature (13–19 °C), the surface cooling, which was stronger during the night, was prolonged into the daytime, causing convection at the surface that penetrated depths gravitationally. This resulted in a vertically homogeneous surface layer with regard to temperature T, salinity S and density σ_T down to a depth of 16 m (Fig. 4, top) at all 31 stations of the near-field. Due to operation in windy weather, there was an uneven distribution of sampling stations (Fig. 9) during this survey, although the near-field area over the diffusers was covered reasonably well.

During the second survey, conducted on a calm morning, temperature at 0.5 m depth was 17.84−19.09 °C, while salinity ranged pronouncedly between 29.46 and 33.26 PSU, which indicated a surface layer of fresher water which limited the penetration of the convection due to surface cooling to the upper 8 m (Fig. 4, bottom). During that period, there was a lot of riverine fresh water over the northern Adriatic which manifested at the places of measurement down to depths 2–8 m.

The pycnocline near the sea-floor in the first survey was governed by the temperature vertical gradient, while the pycnocline near the sea-surface in the second survey was dominated by the salinity vertical gradient (Fig. 4, left). In the first survey, when convection dominated, temperature was decreasing with depth. In the second survey, temperature was increasing with depth in the surface layer of fresher water, while in the layer below it could either increase or decrease with depth, although the density continuously increased. This latter increase, however, does not guarantee stability: temperature and salinity have opposing effects on the vertical density distribution in many parts of the water column, and since heat has a coefficient of molecular diffusivity (=1.5×10^{-3} cm^2/s) for two orders of magnitude larger than that of salt, this favours diffussive convection due to a faster heat exchange in double diffusion processes (Turner, 1973), which is a common phenomena in autumn (Malačič, 1991). Inspection of individual vertical CTD profiles from the second survey shows that some of them have the typical structure of a few successive convective layers. These are driven by heat diffusion, and are separated by the interfaces of a stable density jump due to salinity distribution (staircase distribution), observed at several places in the ocean (Monin and Ozmidov, 1985) (see also the σ_T profile near the sea-floor on the bottom-left plot in Fig. 8). Sharp pycnocline just above the bottom mixed layer in the first field survey migrated vertically by more than 1 m, while in the second survey, the pycnocline near the surface migrated by more than 4 m. The vertical migration was probably caused by internal waves that were trapped in the layer of the sharp density gradient. In the second survey, the front of a freshwater plume was passing the measurement area, since an additional decrease of salinity at the surface was observed during measurements, while the 'major' halocline at depths 4–8 m was present at all 31 stations. The TS diagram (Fig. 4, top right) shows that most of the vertical profiles are stable during the first survey, while the density variations were much larger during the second survey (Fig. 4, bottom right), with the density excess (σ_T) between 21–24 kg/m^3 in the

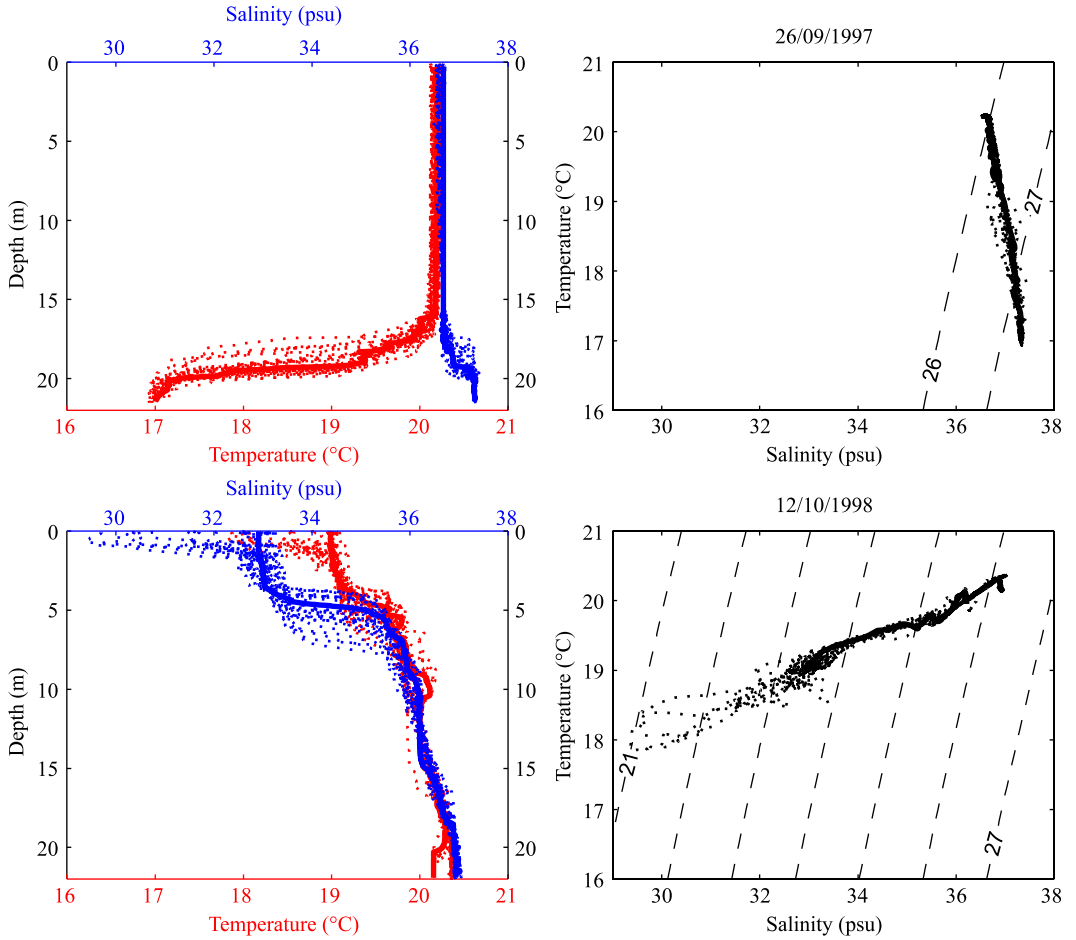

Fig. 4. Temperature and salinity on 26 September 1997 (top), and on 12 October 1998 (bottom): Left: Vertical profiles of temperature and salinity in the near-field. Right: TS diagrams for the same vertical profiles. Dotted lines represent 30 near-field stations, full lines their 'core' central station PI16 (top), or PI11 (bottom), and dashed lines on the right hand plot represent density distribution σ_T.

fresher surface layer, and between 24 and 27 kg/m^3 in the saltier interior.

4.2. Model results of initial dilution

We had to take into consideration that the ambient density varied during the field campaign, and that the spread of effluent depends pronouncedly upon stratification. Fig. 5 (top) shows the vertical profile of horizontally averaged ambient density on 26 September 97, together with the limits of two standard deviations (S.D.) (dotted lines). Since we wanted to capture the least pronounced stratification, as well as the sharpest one, we first composed the least pronounced stratification by adding 2 S.D. of density to the mean in the layers of thickness Δz_L above the pycnocline, and subtracting 2 S.D. in the layers below it. The sharpest stratification was obtained by subtracting 2 S.D. in the layers above the pycnocline and adding 2 S.D. in the layers below it. Then we modified these profiles by considering that the profiles have to be statically stable, which resulted in profiles denoted with dashed lines on Fig. 5 (top). Secondly, variations of initial discharge velocity u_0 had to be accounted for, as described earlier. Simulations were therefore performed for three different values of initial discharge velocity u_0=0.39, 0.45 and 0.55 m/s for

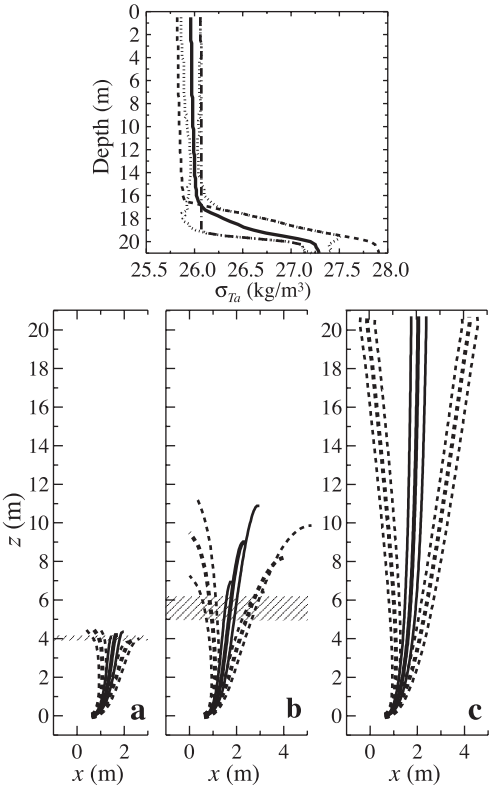

Fig. 5. Top: Vertical distribution of the horizontally averaged density of near-field σ_{Ta} (full line), of averaged values minus 2 S.D. of σ_T, and averaged values plus 2 S.D. of σ_T (dotted), and the distribution of the sharpened density profile with a sharpened pycnocline (dashed) or a weakened pycnocline (dash-dotted line). Bottom: spread of an effluent that emerges horizontally from an orifice of the diffuser when the ambient density profile is (a) that with a sharpened pycnocline; (b) equal to the mean density profile; (c) that with a weakened pycnocline. Full lines: path of the center of the core of an effluent. Dashed lines: envelopes of an effluent where the concentration is 1/e of that in the core's center (at distance r from the core line). Thicker lines: the spread with initial velocity at the orifice u_0=0.45 m/s. Thinner lines: spread with u_0=0.36 m/s (smaller heights), and u_0=0.55 m/s (larger heights). Hatched rectangles mark the area where $\Delta\rho$=0 for three different values of u_0, yet the velocity at those levels is u>0 due to inertia.

the first survey, and u_0=0.6, 0.8 and 1.0 m/s for the second survey.

Since the vertical coordinate of the model increases upward from the height of an orifice, the height of the orifice itself with respect to the sea-bed (of about 1 m) needs to be considered when the plume's height is compared with the depth of the peak of l_T and bacteria. Hatched rectangles on plots (a) and (b) of Fig. 5 (bottom) mark the height interval where the density deficit $\Delta\rho \cong 0$, while on plot (c) with the weakened pycnocline, the plume erupts up to the sea-surface, regardless of the value of u_0. The thickness of the layer in which $\Delta\rho \cong 0$ is questionable. In case (a) of the sharpened pycnocline, the variations of u_0 do not much influence the maximum height of spreading. Since in a layer where $\Delta\rho$=0, the plume has u>0 due to inertia, it is still rising unless the sea-surface has been reached already. After reaching the top of a plume, where u=0, it falls back down towards a depth where $\Delta\rho$=0 (Fischer et al., 1979). The model cannot reproduce this process. In a layer where $\Delta\rho$=0, the ambient advection smears this plume with plumes that originate from other orifices. We may conclude that cases (a) and (b) show that the major concentration of an effluent would range between 5 and 7 m above the sea-floor for the first survey, and that the effluent also occupies the space above these heights. This means that peak concentrations of an effluent were located at depths between 14 and 16 m, where the depth of the sea-floor is around 21 m (mean depth of 20.7 m, and the tidal peak at that time was close to 0.3 m). The uncertainty of these depths is of the order of 1 m. This result agrees with the vertical distribution of l_T and faecal coliforms, as it will be shown.

The dilution factor S varies a great deal with stratification in simulations of the rise of an effluent during the first campaign, since it ranges between 22 and 354, with both limits obtained when the outflow velocity is small, u_0=0.36 m/s. The cone radius that is reached by a single plume before it spreads horizontally is between 2 and 5 m. The larger radius is related to the weak pycnocline case. The whole path of the upward travel of an effluent is completed in less than 2 min.

The same method was applied in the simulations of effluent initial rise and dilution (Fig. 6) for the second survey on 12 October 1998. Since the density profile is more structured, there are more possibilities in composing the strongest and the mildest stratification around the mean profile. It was decided to subtract (add) 2 S.D. at the surface and add (subtract) 2 S.D. to the mean profile to compose the strongest (mildest) stratification. Care was taken to ensure that the density was still increasing with

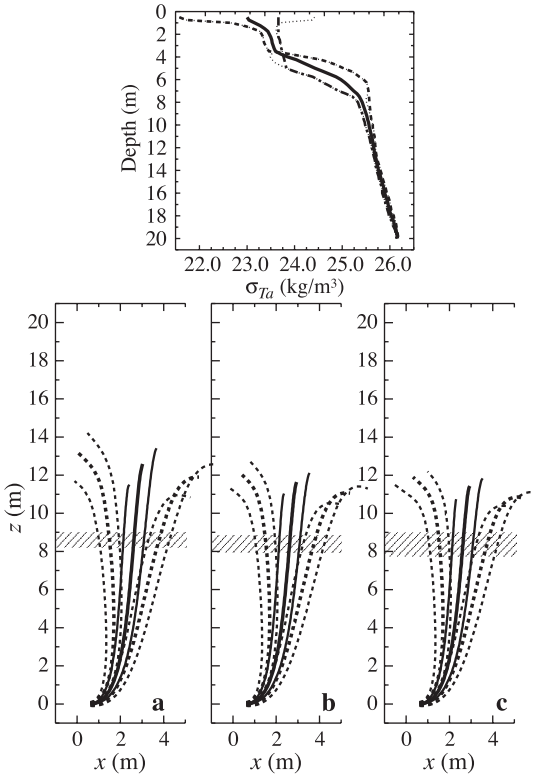

Fig. 6. Same as Fig. 5, except that initial velocity at the orifice has values of 0.6, 0.8 (thicker lines) and 1.0 m/s. The left most figure is for the case with the strongest stratification, and the right most one for the weakest—see text.

depth. All nine simulations (three initial velocities multiplied by three density profiles) gave similar results (Fig. 6, bottom), even with the larger range of initial velocities (0.6, 0.8 and 1 m/s). The run with u_0=2.0 m/s (not shown) also kept the plume below the sea-surface, at a height of around 9.0 m ($\Delta\rho$=0). The results seem to be wrong: for the strongest stratification, the plume heights are the largest when they should be the smallest. They are, however, correct since the mildest (strongest) stratification over the whole water column has the largest (smallest) N in the bottom part of the water column which is what matters in the uplift of the sewage. In all displayed cases, the height at which $\Delta\rho$=0 lies in the interval between 7.9 and 9.0 m, or at depths between 11.7 and 12.8 m. The dilution in simulations of plumes' rise for this second survey is in a much narrower range, between 63 and 68.

4.3. Vertical profile of the overturning length scale

Fig. 7 shows the vertical distribution of displacements that are calculated out from the vertical profiles of T, S and σ_T at station PI16 for the first survey (top) and at station PI11 for the second survey (bottom). These stations were chosen as those at which l_T reaches its maximum (first survey) of all values in the near-field, or a local maximum (second survey) at depth, where it is expected from the numerical model that the sewage would spread horizontally. One observes that in the upper part of the overturning patches, the displacements are negative (downwards), while in the lower part of the water column they are positive (upwards). At station PI16 (first survey), the expected overlapping of three types of displacement (calculated from the profiles of T, S and σ_T) does not show very distinct differences among them. There are depths at which displacements are of one type only. A large convective cell expands from the surface down to a depth of 16 m, and is modified at its bottom by the rising sewage. This results from the salinity wiggles at that depth (top left plot). The situation is quite different at station PI11 of the second survey. One observes several patches of displacement (Fig. 7, bottom right), the density profile generated six patches, the largest of them expanded between 11 and 14.5 m. The displacement profile calculated from the salinity profile is covered by displacements of the density profile. Complete overturn of the water column would be obtained if only temperature affected the density.

Fig. 8 displays relative agreement between the vertical distribution at station PI16 of bacteria (faecal coliform, FC), and of l_T (top left plot) of the first survey, both distributions peak at 16-m depth, just above the sharp pycnocline, where FC=1680/100 ml, and l_T=14 m. Pre-averaging of σ_T over Δz_a=1.0 causes the peak of l_T to be wider and centered around a shallower depth (15 m), and pre-averaging over $\Delta z_a \leq$ 0.5 m did not improve the match with bacterial distribution—which has a vertical resolution of 1 m at most. The top right plot of Fig. 8 displays the vertical distribution of horizontal statistics in layers of Δz_L=0.25 m. While minima over all 31 stations of the near-field are close to zero except for the near-surface 4 m, the vertical distribution of the average of l_T over 31

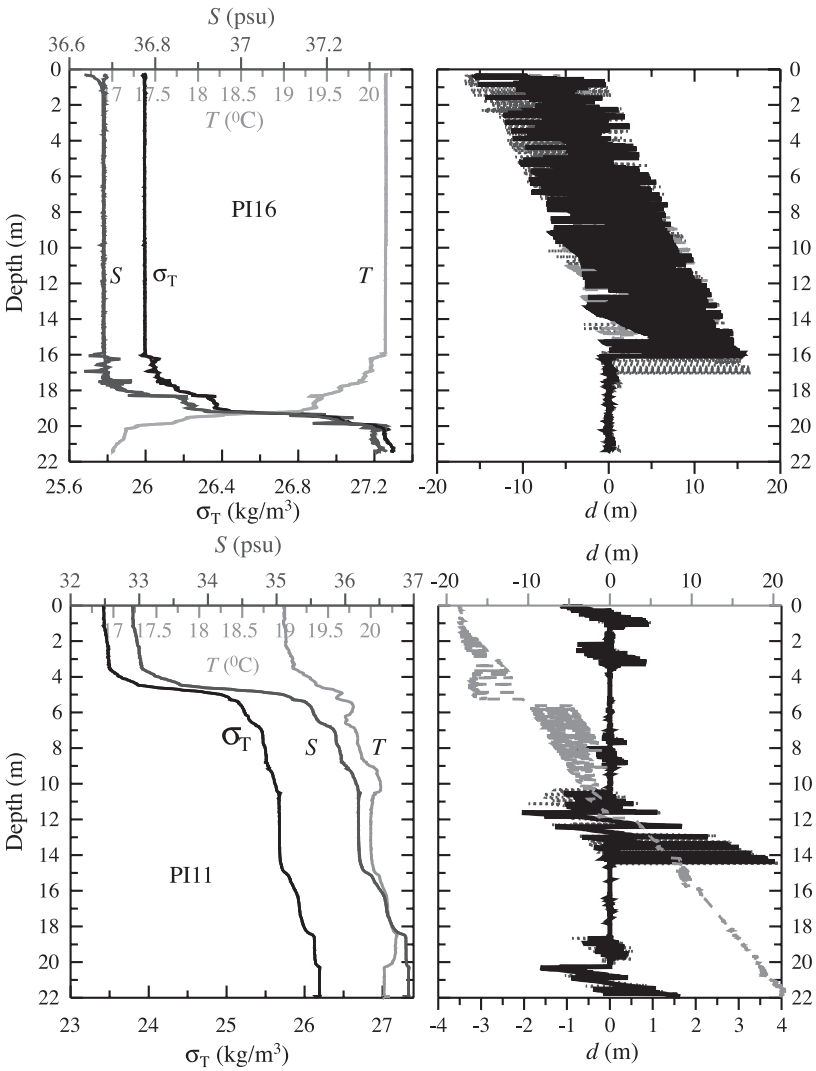

Fig. 7. Top: vertical profiles of T (grey), S and σ_T at station PI16 of the near-field (left) on 26 September 1997. Thick lines represent measured profiles, thin lines, which are mostly covered by thick ones, represent profiles of sorted particles in which T decreases with depth, while S and σ_T increase. Right: corresponding profiles of the displacements d, calculated from profiles of T (dashed grey), S (dotted grey) and σ_T (full black), except that there is no thin line of ordered particles for temperature. Bottom: same profiles for station PI11 on 12 October 1998. The scale for d calculated from the T profile is at the top of the right bottom plot, while the scale for d calculated from the σ_T and S profile is at the bottom of this plot.

stations does not show a significant peak. The average decreases at depths between 15 and 16 m, below which there is no overturning turbulence. Vertical distribution of the maxima of l_T, however, shows a peak, again located at 16-m depth. No pre-averaging was applied here on σ_T profile.

The situation of the second survey at PI11 differs from the first in that FC has a much broader peak between 11.0 and 16.7 m, with values larger or equal to 265/100 ml, and a maximum recorded value of 460,100 ml at a depth of 16 m. The sampling resolution was poor, however, we may say that the layer with a larger faecal load begins with a sharp increase from zero at 10.6 m to 265/100 ml at 11.0 m, and ends with an abrupt decrease from 365/100 ml at 16 m to 5/100 ml at 18 m (zero at 18.5

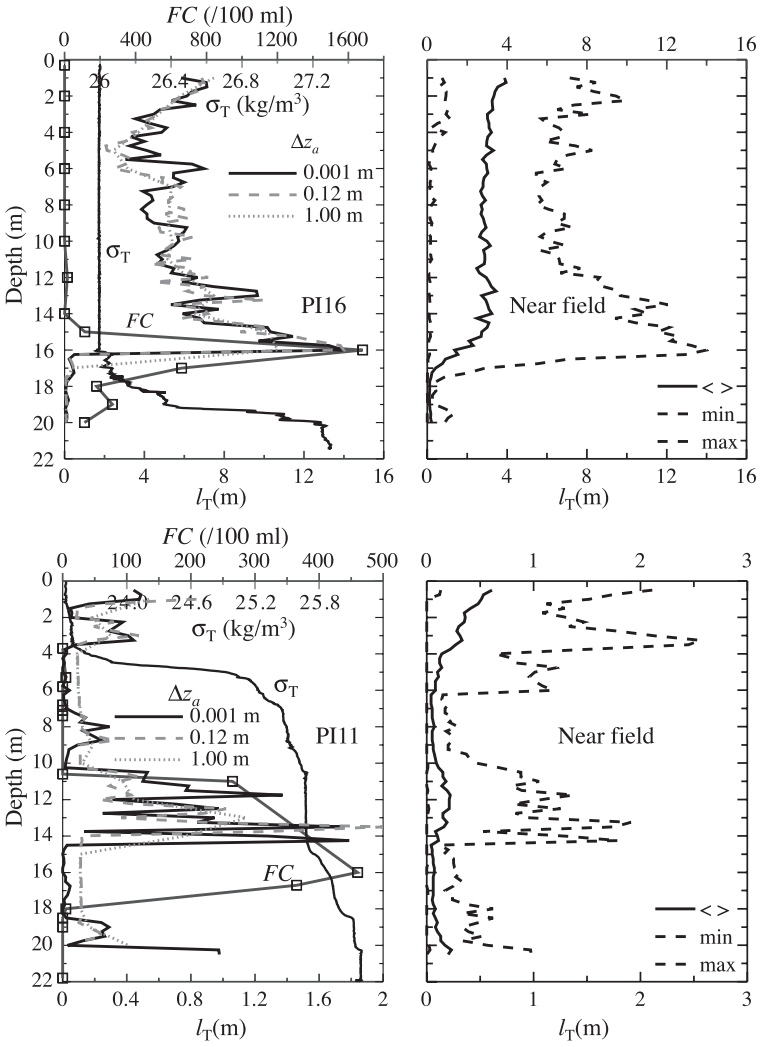

Fig. 8. Left plots: vertical distribution of faecal coliforms (FC), density σ_T and l_T of this density profile for three values of the pre-averaging interval Δz_a at station PI16 on 26 September 1997 (top), and at station PI11 on 12 October 1998 (bottom). Right plots: Vertical distribution of the horizontal average, the horizontal minima and maxima of l_T of σ_T of the whole near-field (31 stations) of the first cruise (top), and of the second (bottom). On all plots Δz_L=0.25 m.

m depth). The vertical profile of l_T roughly follows the profile of bacteria, having a few peaks between 11.0 and 16.7 m, that are merged into one when the pre-averaging of the density profile is performed with a window of 1 m. There are some overturning activities in the fresher surface layer down to 4 m, and above the sea-floor, below depths of 18.5 m. Statistical distribution of l_T (bottom right) confirms that in the surface layer there is a maximum (at another station) that is larger than the one observed at PI 11 at depth, where larger values of l_T and FC are located, and to which sewage should rise according to the model. There is a relatively thick layer of double diffusion, which except for a small and narrow density spike at its top at a depth of 11.5 m is otherwise homogeneous down to 14.5 m. At depths below 18.0 m, two other, even more typical figures of the density profile of diffusive convection are evident, similar to those observed in oceans (Monin and Ozmidov, 1985; Turner, 1973).

4.4. Space distribution of the overturning length scale

It follows from the vertical profile of different quantities at station PI16 that the horizontal distribution of quantities found at a depth of 16 m during the field campaign on 26 September 1997 seems interesting. It also follows from the profile at station PI11 of the second campaign on 12 October 1998, that at a depth of 13.5 m there is a larger variation of l_T. Fig. 9 shows that on 26 September 1997 at 16.0 m depth, the temperature of sea-water is slightly higher around the diffusers and that salinity is slightly lower, although this distinction between 'fresher' and 'saltier' water mass is not that clear and they do not correlate much except around diffusers. That is why the density field is slightly lower at that depth around station PI16. Among the horizontal variations of T, S, σ_T and l_T, the variation of l_T is the most pronounced: it reaches values that are for an order of magnitude (10 m) higher between the diffusers than those at the edge of the near-field zone (1 m).

Data analysis shows that during the first survey, temperature at a depth of 16 m varies for 0.17 °C (S.D.=0.04 °C), salinity for 0.07 PSU (S.D.=0.01), and density for 0.09 kg/m^3 (S.D.=0.02 kg/m^3), just above the ambient 'noise level', which is estimated to be around 0.02 for all three quantities in relevant units. Their relative changes with respect to their maximum value are in the range between 2×10^{-3} (salinity) and 8×10^{-3} (temperature), or 0.8% at most, if for the density σ_T is applied. Contrary to that, respective

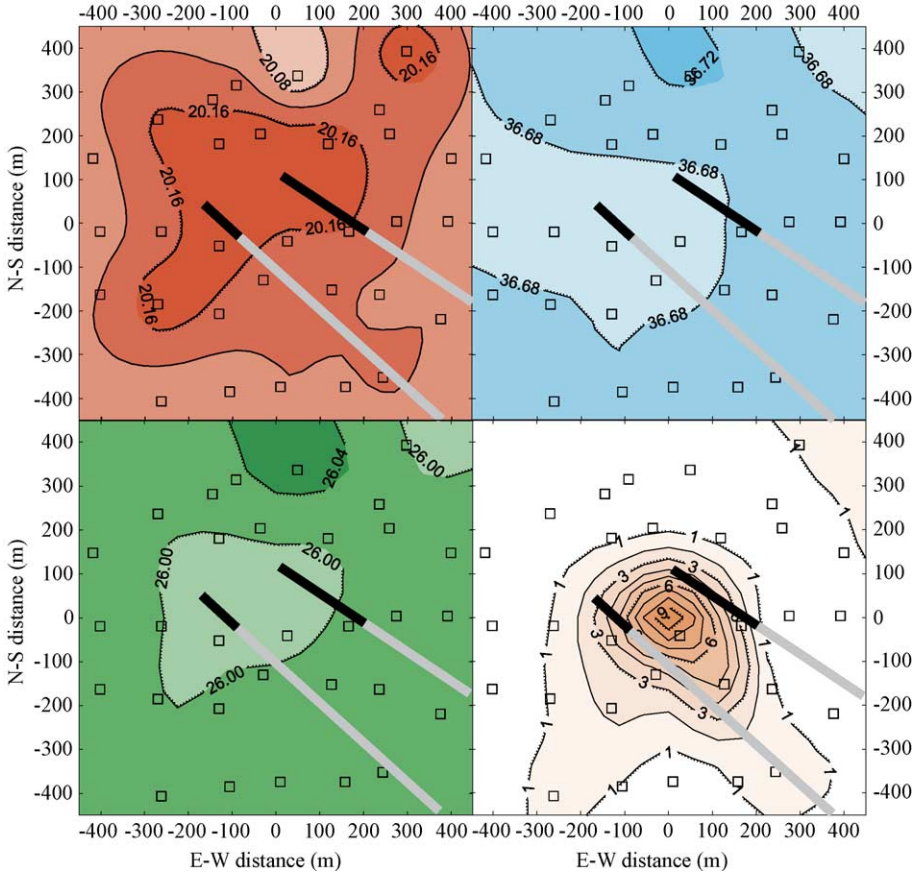

Fig. 9. Horizontal distribution of T (top left), S (top right), σ_T (bottom left) and l_T (bottom right) at a depth of 16 m on 26 September 1997. Dark and gray straight lines mark the diffusers and pipes in a simplified way, small rectangles mark the positions where casts were made. Values of isolines of T, S and σ_T are separated for 0.04 in relevant units, while isolines of l_T differ for 1.0 m. E–W and N–S distance is measured from the center of the near-field (see Fig. 2). The Kriging interpolation procedure was applied, where the grid lines were separated for 112.5 m.

relative changes of the overturning length scale, which varies between 0.1 and 13.9 m at that depth (S.D.=2.7 m, average 1.4 m), are about 99%. In this case, the method here described for the detection of turbulent alien water would therefore increase the 'sensibility of the detection method' with respect to the temperature and salinity fields more than 120 times, and more than 1200 times if the relative variations with respect to the mean values are considered.

On 12 October 1998 at a depth of 13.5 m, the situation is very different (Fig. 10): temperature and salinity are roughly increasing from the NW corner of the measurement area towards the diffusers, although this trend is not that clear for salinity. There is a smaller pool of lighter (and fresher) water in front of the smaller (left-hand) diffuser, around station PI11, where a local peak of l_T is centered with a value smaller than 2.0 m. Analysis of the data from this second survey shows that at depth of 13.5 m, around which the peak of bacteria was detected and which is close to the level up to which the sewage plumes should rise, temperature varied for 0.22 °C (S.D.=0.04 °C), which is similar to the horizontal variations in the first survey. The salinity, however, varied for 0.21 PSU (S.D.=0.06), and the density for 0.14 kg/m^3 (S.D.=0.04 kg/m^3). Relative changes of all three quantities with respect to their maximum value are between 0.5% and 1.1%. The overturning length scale varies between 0.0 and 1.7 m at that depth (S.D.=0.32 m, average 0.16 m), the relative change is of 100%, which is about 91–200 times larger than those of T, S, and σ_T.

The vertical plane in an E–W direction that passes through the center of the near-field (Fig. 11) shows a vague distribution of σ_T in a layer above 15 m depth

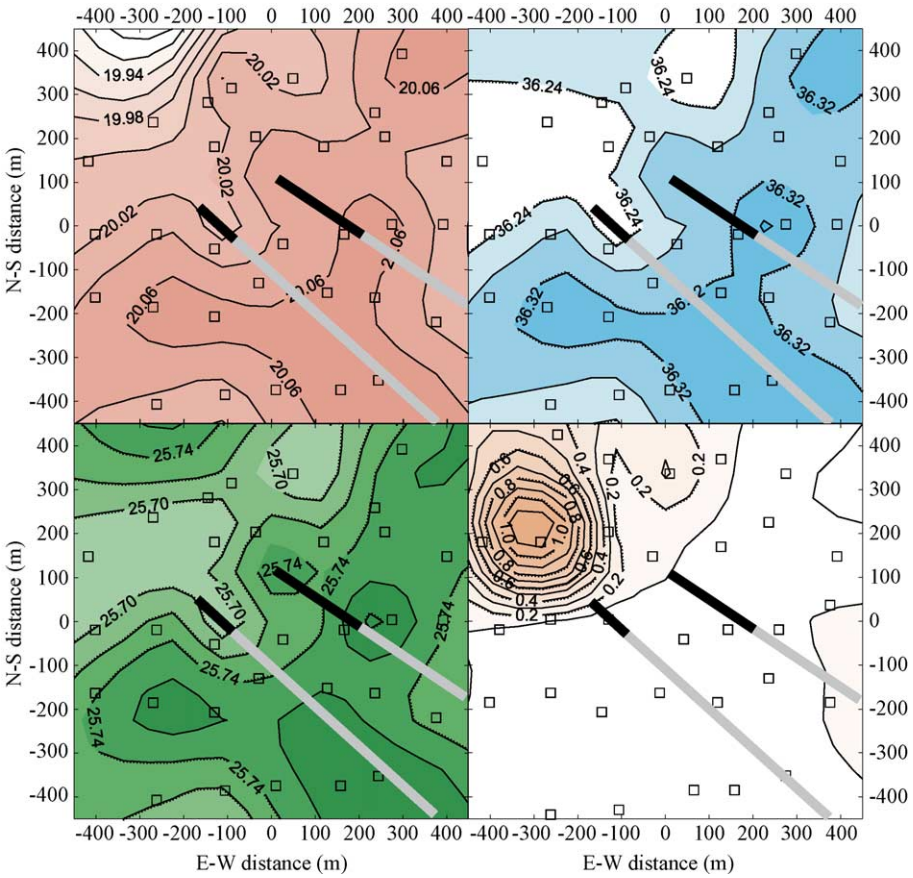

Fig. 10. Same as in Fig. 9, except for the depth of 13.5 m on 12 October 1998. Values of isotherms are separated for every 0.04 °C, isohalines for 0.02 PSU, isolines of σ_T differ for 0.02 kg/m^3, and of l_T for 0.1 m.

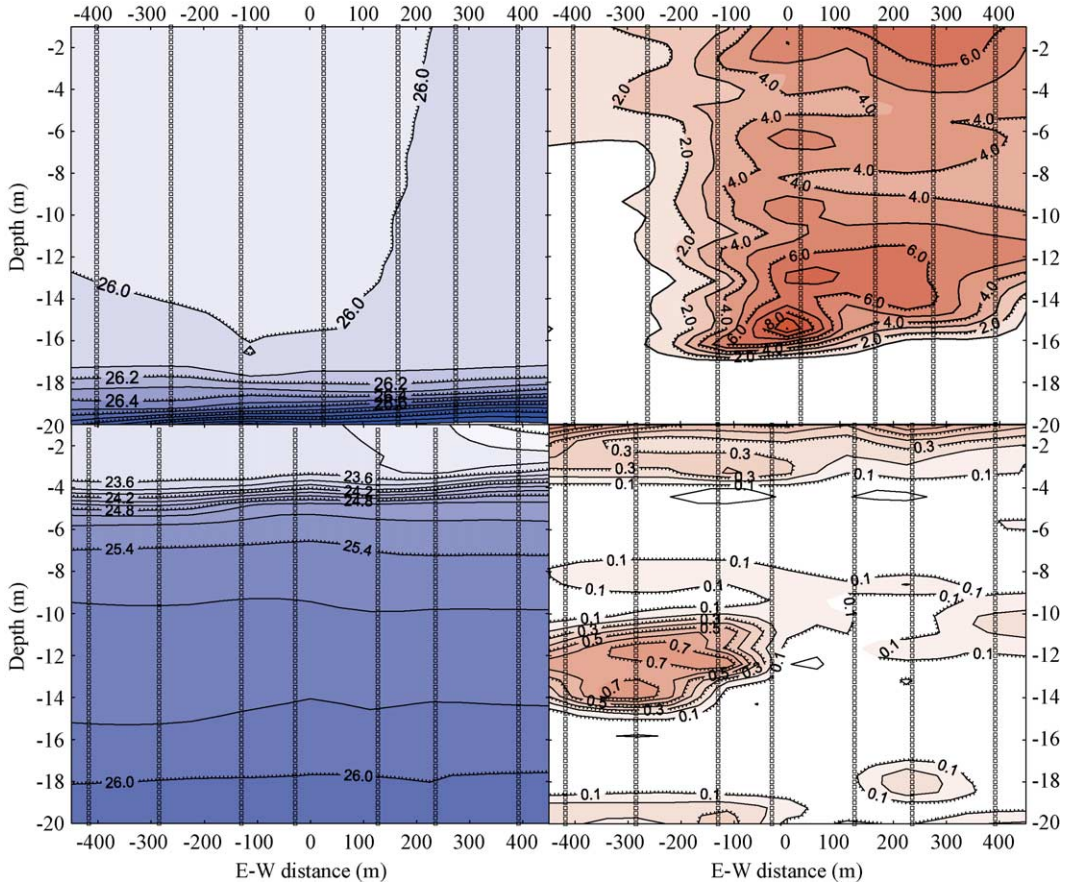

Fig. 11. Distribution of σ_T (left) and of l_T (right) in a vertical plane that spreads in an E–W direction and passes through station PI16 (see Fig. 2) on 26 September 1997 (top), and through station PI11 on 12 October 1998 (bottom). Isolines of σ_T differ by 0.1 kg/m^3 and of l_T by 1.0 m (top), or by 0.2 kg/m^3 and 0.1 m, respectively (bottom). Small rectangles denote values that were applied in space Kriging interpolation, where the horizontal weight scaled against the vertical for a factor of 100. Horizontal grid lines were separated for 112.5 m, while the vertical lines differed for 0.76 m.

(top left) on 26 September 1997, a lighter (slightly warmer and fresher) water mass eastward, and a pronounced increase of σ_T (decrease of T and increase of S) at depths below 15 m. The distribution of the overturning length scale is very pronounced (top right). It varies for an order of magnitude and indicates that all plumes that emerge from 25 orifices of two diffusers are merged together, mostly by ambient currents. They form a large plume that extends horizontally and vertically above a depth of 17 m, with a core between the diffusers and a tail, which is 1 m higher than the core (depth 16 m) and spreads westward. The core is at a depth where a higher amount of FC was found and which is also the greatest depth (smallest height) up to which the effluent should rise according to the model. A similar plot would be obtained in a vertical plane in the N–S direction, where the tail of an effluent would spread northward. This is in accordance with the most recent ADCP current-meter observations of the coastal oceanographic buoy which is less than 2 km away from the diffusers in a NE direction. They show a counter-current at depths during bora wind episodes (unpublished records). This pattern was recently confirmed with numerical simulations of the circulation of the Gulf of Trieste, performed by the Princeton Ocean Model that is nested in another model of the northern Adriatic Sea (unpublished results of the ADRICOSM project).

In Fig. 11 (bottom), the situation on 12 October 1998 is displayed in an E–W vertical plane that passes

through station PI11. There is a fresher water mass above 4 m depths on the western side of the measurement's domain. A significant overturning potential is present in this surface layer. In depths between 10.5 and 14.5 m, a localized region of larger l_T spreads from the eastern (left-hand) side of the domain towards the center. To these depths, a sewage plumes should rise according to the model (within 1 m error) and a larger amount of FC was there detected at station PI11.

5. Discussion

The applied numerical model of initial dilution that simulates the vertical spread of sewage that emerges from the diffusers' orifices is grounded on the hypothesis that the ambient turbulence is negligible. This is far from reality when wind forcing and convective overturns are present in a shallow sea, since these processes erode the stratification and thus enhance the overturning length scale of the ambient into which the fluid in question enters. However, the distribution of l_T indicates that the water column was turbulent above a depth of 16 m during the first survey. There was diffusive convection that overturned the surface fresh water and water mass at depth at some localized places during the second survey. This latter activity was horizontally more non-homogeneous. The condition of low ambient turbulence, required by the model of initial upward spread of an effluent, could be satisfied in a layer between depths of 16 and 21 m during the first CTD campaign, and between 14 and 21 m during the second one.

Most (ecological) research groups lack CTDs that have a fast response and whose falling speed is high (of an order of 1 m/s), but have CTDs with a much lower falling speed, as well as a slow sampling rate (Zhang, 1994), and are still estimating the overturning length scale. This means that surveys of this kind are possible but require careful design, especially when it is expected that the flow rate of the source of the fluid in question varies quickly, on an hourly basis, as was the case in the campaign described here (Malačič, 2001), when between 6 AM and 8 AM the outflow rate increased from about 70 to over 115 l/s during the first survey, and varied between 136 and 192 l/s during the second survey. This variability in flow rate could also generate separate blobs of an effluent that are similar to each other yet distinct from ambient water. Created at different times, they mostly travel in different directions, according to advection at the depth of neutral buoyancy.

Closer inspection of vertical CTD profiles showed that, quite frequently, small wiggles on temperature and salinity profiles occurred mostly, but not exclusively, at depths with sharper vertical gradients of temperature and salinity. Later analysis leads us to the conclusion that some of the wiggles were a consequence of the drop speed of CTD casts that was too high for a proper match between temperature and conductivity sensors. This results in salinity and density spiking. However, many of the wiggles could not be explained in this way. The dynamic response of the fine-scale FPS2 probe was carefully studied by the University of Western Australia (Fosdar et al., 1985). Their method improves the output of the Sea-Bird sensors by using sharpening/smoothing software. In their study, the rms of the displacements were also presented (their Fig. 15) for the uncorrected and corrected (smoothed and sharpened) temperature signal. The difference is obvious, and the corrected signal gave a much higher overturning length scale in a region where the water column was statically not very stable (small N^2). It follows that the 3D distribution of the displacement around the diffusers in the survey here described would be masked by the sensors' output without the software sharpening, since the falling speed of the probe was relatively high, and the difference in the sensors' response then is amplified. There are other factors related to instrument fault, such as the thermal inertia of the temperature probe, and of the conductivity cell (Lueck and Picklo, 1990; Morison et al., 1994).

In both CTD surveys, the distribution of enhanced l_T around the level of neutral buoyancy of an effluent resembles the one that has been observed for the spread in a cross flow in laboratory experiments (Akar and Jirka, 1995; Roberts et al., 1989a; Roberts et al., 1989b), and also some field observations of the spread of a dye (Peeters et al., 1996), where the head of its concentration is located at the point of release, and a wider tail spreads with currents. The vertical profile of the peak of the beam attenuation coefficient at 660 nm around a sewage plume at Sand Island, Hawaii (Petrenko et al., 1997) also resembles the vertical

profiles of l_T and FC that were described here. The shape of some strange TS lines (Fig. 4), however, was examined in another study (Petrenko et al., 1998) which revealed that the mixing of ambient fluid with the effluent modifies the TS diagrams.

The problem with the hypothesis that the overturning length scale l_T could be the appropriate measure for the spread of a fluid (pollutant) of interest lies in the fact that in most cases, the ambient fluid already has a layered structure of turbulence. This manifests in the vertical distribution of l_T, without the injection of a turbulent pollutant. Moreover, the fluid which is to be detected reaches a neutral buoyancy quite frequently at a level just above the sharp pycnocline, where shear instabilities are frequent and instabilities like those of the Kelvin–Helmoltz type (Thorpe, 1977) or other internal wave structures and wave–wave interactions (Saggio and Imberger, 2001) break and generate turbulent patches. These phenomena are not distributed just over a limited range around the source of the emergence of an alien fluid. If the horizontal and vertical distribution of l_T around the fluid source shows a limited domain of distribution of l_T that is decreasing with the distance from the source, then l_T could serve as a clear indicator of the source of a fluid that is more turbulent than the ambient one. However, new CTD surveys with a released dye and current meter observations are required to confirm this hypothesis.

Relative changes of l_T that are larger than respective changes of T, S, and σ_T for several orders of magnitude show a relatively low improvement in sensitivity when compared with some tracer methods, but considering costs and benefits, an estimate of turbulent fluid just from l_T, that is calculated from measurements with the same sensors, seems to be efficient enough. The problem is to confirm that variations of l_T could be attributed to an alien fluid alone. Also for this, a survey with a dye needs to be undertaken.

We also have to be careful about the 'ambient noise' of l_T. The frequency distribution of 31 values of l_T on 26 September 1997 at a depth of 16 m in bins of 1.0 m shows huge asymmetry: 22 of them are smaller than 1.0 m, 4 are between 1.0 and 2.0 m, 5 above 2.0 m, and 3 are above 4.0 m. Higher values are all located around the center of the near-field and decrease outwards. Values of l_T on 12 October 1998 are also asymmetrically distributed around the mean value at a depth of 13.5 m: three of them are lower than 0.2 m, 24 in the range 0.2–0.4 m (average value), four above 0.4 m, and only one is between 1.6 and 1.8 m. Higher values were located around the front end of the left diffuser. We may say that the ambient noise of l_T is below 1 m in the first survey and that more than 38% of values are above the ambient fluctuations of l_T. If for the second survey the ambient noise is defined as the one with $l_T<0.2$ m, only four values (13%) are above this level, and the l_T field is more doubtful as the representative one for the detection of an alien fluid.

This also leads to a discussion related to the aliasing, or space-resolution problem. Since the supposed grid of stations has a resolution between 130 m (E–W direction) and 185 m (N–S direction), while in-situ measurements could have larger and smaller ranges, we may estimate that structures with horizontal dimensions smaller than 300 m are poorly captured by the space interpolation method (Kriging), where grid lines were horizontally separated for 112.5 m as a compromise between the resolution and the number of grid values (nine of them). This means that structures like narrow 'chimneys' of convection along which the water turns down could not be resolved. Nonetheless, the 'core' area of five values of $l_T>2$ m which corresponds to larger values of temperature, lower values of salinity and higher values of density around station PI16 during the first cruise is firmly revealed, even if its boundary with the rest of the near-field is not properly represented. Along the vertical, the space resolution of measurements is more than sufficient.

6. Conclusion

Model results of the initial rise of an effluent plume that originates from diffusers at the sea-floor are in reasonable agreement with the location of faecal load in the water column above them. Although wind-driven mixing and convection due to heat loss in the first survey, and diffusive convection due to double diffusion of heat and salt in the second survey affected the overturning length scale, the position of one of the local peaks of the overturning length scale calculated from the density profile in the core of the sewage near-field matches with the position of the peak of

vertical distribution of the faecal coliforms, and with the height of the simulated plume rise.

It is easy to implement the method of the overturning length scale on board a vessel right after the CTD casts. Despite its faults, the method offers a prospective means to the first estimate of the source of a different water mass in lakes, reservoirs and coastal seas. In addition to the analysis of a spread of sewage that emerges from submarine diffusers, it could be applied in studies where tongues of intrusion of another water mass are to be detected, such as those that originate from underground sources on side-banks or floors, or river inflows with a density higher than the ambient one, or where the flow from undersea freshwater springs is to be determined. It looks as if the local maximum of the overturning length scale is a necessary, but not a sufficient condition for finding an alien turbulent water mass. Since the field of the overturning length is affected by different mechanisms, sufficient care must be taken in the analysis of the overturning field. It is expected that a match can be found between the position of a peak of the overturning length scale and the location at which the fluid in question spreads horizontally and this can narrow the search area for an alien fluid. The correlation, however, could occur in coastal waters only for an overturning length scale that is calculated from a density profile.

Acknowledgements

The author is indebted to Prof. S. Thorpe for the valuable discussions, to V. Turk for the analysis of bacteria, to A. Vukovič for the precious help in field-surveying and T. Makovec for the assistance.

References

Akar, P.J., Jirka, G.H., 1995. Buoyant spreading processes in pollutant transport and mixing: Part 2. Upstream spreading in weak ambient current. J. Hydraul. Res. 33 (1), 87–100.

Anon, 1992. A field measurement system for mixing and biological investigations. WP 602 DL, Centre for Water Research. University of Western Australia, Perth.

Avčin, A., Vrišer, B., Vukovič, A., 1979. Ecosystem modifications around the submarine sewage outfall from Piran sewage system. Slovensko morje in zaledje (in Slov.) 2–3, 281–299.

Brubaker, J.M., 1987. Similarity structure in the convective boundary layer of a lake. Nature 330 (24), 742–745.

D' Asaro, E.A., Dairiki, G.T., 1997. Turbulence intensity measurements in a wind-driven mixed layer. J. Phys. Oceanogr. 27, 2009–2022.

Dillon, M.T., 1982. Vertical overturns: a comparison of Thorpe and Ozmidov length scales. J. Geophys. Res. 87 (C12), 9601–9613.

Etemad-Shahidi, A., Imberger, J., 2001. Anatomy of turbulence in thermally stratified lakes. Limnol. Oceanogr. 46 (5), 1158–1170.

Faganeli, J., 1982. Nutrient dynamics in seawater column in the vicinity of Piran submarine sewage outfall (North Adriatic). Mar. Pollut. Bull. 13, 61–66.

Fan, L.N., Brooks, N.H., 1966. Horizontal jets in stagnant fluid of other density. J. Hydraul. Div.-ASCE 92 (HY2), 423–429.

Featherstone, R.E., 1984. Mathematical models of the discharge of wastewater into a marine environment. In: James, A. (Ed.), An Introductory to Water Quality Modelling. John Wiley, Chichester, pp. 150–162.

Fer, I., Lemmin, U., Thorpe, S.A., 2002. Contributions of entrainment and vertical plumes to the winter cascading of cold shelf waters in a deep lake. Limnol. Oceanogr. 47 (2), 576–580.

Fischer, H.B., List, E.J., Koch, R.C.Y., Imberger, J., Brooks, N.H., 1979. Mixing in Inland and Coastal Waters. Academic Press, New York. 483 pp.

Flór, J.B., Fernando, H.J.S., van Heijst, G.J.F., 1994. The evolution of an isolated turbulent region in a two-layer fluid. Phys. Fluids 6 (1), 287–296.

Fonseka, S.V., Fernando, H.J.S., van Heijst, G.J.F., 1998. Evolution of an isolated turbulent region in a stratified fluid. J. Geophys. Res. 103 (C11), 24857–24868.

Fosdar, F.M., Parker, G.J., Imberger, J., 1985. Matching temperature and conductivity sensor response characteristics. J. Phys. Oceanogr. 15, 1557–1569.

Imberger, J., Hamblin, P.F., 1982. Dynamics of lakes, reservoirs, and cooling ponds. Annu. Rev. Fluid Mech. 14, 153–187.

Lueck, G.R., Picklo, J.J., 1990. Thermal inertia of conductivity cells: observations with a Sea-Bird cell. J. Atmos. Ocean. Technol. 7, 756–768.

Malačič, V., 1991. Estimation of the vertical eddy diffusion coefficient of heat in the Gulf of Trieste (Northern Adriatic). Oceanol. Acta 14 (1), 23–32.

Malačič, V., 2001. Numerical modelling of the initial spread of sewage from diffusers in the Bay of Piran (northern Adriatic). Ecol. Model. 138, 173–191.

Malačič, V., Viezzoli, D., 2000. Tides in the northern Adriatic Sea—the Gulf of Trieste. Nuovo Cim. 23 (C4), 365–382.

Malačič, V., Vukovič, A., 1997. Preliminary results of the submarine outfall survey near Piran (northern Adriatic Sea). In: Kranjc, A. (Ed.), Tracer Hydrology, vol. 97. Balkema, Portorož, pp. 263–268.

Malačič, V., Petelin, B., Vukovič, A., Potočnik, B., 2000a. Municipal discharges along the Slovenian littoral (the northern Adriatic Sea)—community planning and the environmental load. Period. Biol. 102 (Suppl. 1), 91–100.

Malačič, V., Viezzoli, D., Cushman-Roisin, B., 2000. Tidal dynamics in the northern Adriatic Sea. J. Geophys. Res. 105 (C11), 26265–26280.

Malej, A., 1980. Effects of Piran underwater sewage outfall upon surrounding coastal ecosystem (North Adriatic). Journées Étud. Pollutions C. I. E. S. M., Cagliari, Italy, 743–748.

Monin, A.S., Ozmidov, R.V., 1985. Turbulence in the Ocean. D. Reidel Publishing, Dordrecht, pp. 267.

Morison, J., Andersen, R., Larson, N., D'Asaro, E., Boyd, T., 1994. The correction for Thermal-lag effects in Sea-Bird CTD data. J. Atmos. Ocean. Technol. 11, 1151–1164.

Mozetič, P., Malačič, V., Turk, V., 1999. Ecological characteristics of seawater influenced by sewage outfall. Annales 9 (2), 177–190.

Oakey, N.S., Elliott, J.A., 1982. Dissipation within the surface mixed layer. J. Phys. Oceanogr. 12, 171–185.

Ogrin, D., 1995. Clima of Slovenian Istra. Zgodovinsko društvo za Juno Primorsko. Koper, 381 pp. (in Slov.).

Olivotti, R., Faganeli, J., Malej, A., 1986. Impact of 'organic' pollutants on coastal waters, Gulf of Trieste. Water Sci. Technol. 18, 57–86.

Peeters, F., Wüest, A., Piepke, G., Imboden, D.M., 1996. Horizontal miixing in lakes. J. Geophys. Res. 101 (C8), 18361–18375.

Petrenko, A.A., Jones, B.H., Dickey, T.D., LeHaitre, M., Moore, C., 1997. Effects of a sewage plume on the biology, optical characteristics, and particle size distributions of coastal waters. J. Geophys. Res. 102 (C11), 25061–25071.

Petrenko, A.A., Jones, B.H., Dickey, T.D., 1998. Shape and initial dilution of Sand Island, Hawaii sewage plume. J. Hydraul. Eng.-ASCE 124 (6), 565–571.

Press, W.H., Teukolsky, S.A., Vetterling, W.T., Flannery, B.P., 1992. Numerical Recipes in Fortran, 2nd ed. Cambridge University Press, Cambridge, USA, pp. 963.

Roberts, P.J.W., Snyder, W.H., Baumgartner, D.J., 1989a. Ocean Outfalls: II. Spatial evolution of submerged wastefield. J. Hydraul. Eng.-ASCE 115 (1), 26–47.

Roberts, P.J.W., Snyder, W.H., Baumgartner, D.J., 1989b. Ocean Outfalls: III. Effect of diffuser design on submerged wastefield. J. Hydraul. Eng.-ASCE 115 (1), 49–70.

Saggio, A., Imberger, J., 2001. Mixing and turbulent fluxes in the metalimnion of a stratified lake. Limnol. Oceanogr. 43, 1780–1795.

Sherwin, T.J., Jonas, P.J., 1994. The impact of ambient stratification on marine outfall studies in British waters. Mar. Pollut. Bull. 28 (9), 527–533.

Sherwin, T.J., Jonas, P.J., Sharp, C., 1997. Subduction and dispersion of a buoyant effluent plume in a stratified English Bay. Mar. Pollut. Bull. 34 (10), 827–839.

Thorpe, S.A., 1977. Turbulence and mixing in a Scottish Loch. Philos. Trans. R. Soc. Lond., A 286 (A), 17–181.

Thorpe, S.A., 1995. Dynamical processes of transfer at the sea surface. Prog. Oceanogr. 35, 315–351.

Turner, J.S., 1973. Buoyancy Effects in Fluids. Cambridge University Press, London, pp. 367.

Turner, J.S., 1986. Turbulent entrainment: the development of the entrainment assumption, and its application to geophysical flows. J. Fluid Mech. 173, 431–471.

UNESCO, 1988. The acquisition, calibration, and analysis of CTD data. A report of SCOR Working Group 51. 54, Unesco Technical Papers in Marine Science, Unesco, Paris.

Vollmer, M.K., 1991. Sharpening and matching response signals for finescale sensors. WP 630 MV, Centre for Water Research. University of Western Australia, Perth.

Washburn, L., Jones, B.H., Bratkovich, A., Dickey, T.D., Chen, M.-S., 1992. Mixing, dispersion and resuspension in vicinity of ocean wastewater plume. J. Hydraul. Eng.-ASCE 118 (1), 38–58.

Wu, Y., Washburn, L., Jones, B.H., 1994. Buoyant plume dispersion in a coastal environment: evolving plume structure and dynamics. Cont. Shelf Res. 14 (9), 1001–1023.

Zhang, S., 1994. Dynamics of Vertical Mixing in Lake Geneva: Overturning Scales and Energetics. École Polytechnique Fédérale de Lausanne, Lausanne, 209 pp.